molecular pharmaceutics

articles

Quantitative CT Imaging of the Spatial and Temporal Distribution of Liposomes in a Rabbit Tumor Model

Jinzi Zheng,[†,‡,§] David Jaffray,[†,‡,§,∥] and Christine Allen*[,§,⊥]

Department of Medical Biophysics, University of Toronto, Toronto, Ontario, Canada, Department of Radiation Physics, Radiation Medicine Program, Princess Margaret Hospital, University Health Network, Toronto, Ontario, Canada, STTARR Innovation Centre, Radiation Medicine Program, Princess Margaret Hospital, University Health Network, Toronto, Ontario, Canada, Department of Radiation Oncology, University of Toronto, Toronto, Ontario, Canada, and Faculty of Pharmaceutical Sciences, University of Toronto, Toronto, Ontario, Canada

Received November 14, 2008; Revised Manuscript Received February 3, 2009; Accepted February 4, 2009

Abstract: Successful employment of noninvasive imaging techniques to quantitatively assess the *in vivo* pharmacokinetics and biodistribution of nanoparticle drug delivery systems will facilitate the rational design of novel targeted drug carriers. This study reports on the bulk organ/tissue (liver, kidneys, spleen, tumor and blood) and intratumoral distribution of liposomes containing iohexol and gadoteridol over a 14-day period in VX2 sarcoma-bearing New Zealand White rabbits using computed tomography (CT). The vascular half-life of the liposomes was found to be 63.6 ± 5.8 h and the maximum tumor-to-muscle iodine concentration ratio of 11.9 ± 6.0 was measured 7 days postinjection with 1.13 ± 0.29% ID of liposomes accumulating at the tumor site. The liposomes achieved their highest intratumoral distribution volume ratio at 48 h postadministration, occupying 72 ± 5% of the total tumor volume. This investigation demonstrated the feasibility of using CT to perform quantitative, volumetric and longitudinal assessment of the pharmacokinetics and biodistribution of iodinated liposomes with sensitivities in the range of $\mu g/cm^3$ while maintaining the ability to identify boundaries of anatomical structures at submillimeter resolution and with imaging time of less than one minute per scan. If successfully approved for clinical adoption, the use of CT imaging to monitor nanoparticulate drug delivery will provide an opportunity for online adjustment of therapeutic regimens and implementation of personalized medicine.

Keywords: Computed tomography; liposome; pharmacokinetics; biodistribution; drug delivery; imaging

Introduction

Characterization of the pharmacokinetics and biodistribution of novel imaging and therapeutic agents is critical for understanding their potential performance and effectiveness *in vivo*.[1−4] In recent years, developments in imaging techniques have provided new tools for noninvasive visu-

* Corresponding author: Dr. Christine Allen, Faculty of Pharmaceutical Sciences, University of Toronto, 144 College Street, Toronto, Ontario, Canada M5S 3M2. Tel: (416) 946-8594. Fax: (416) 978-8511. E-mail: cj.allen@utoronto.ca.

† Department of Medical Biophysics, University of Toronto.

‡ Department of Radiation Physics, Radiation Medicine Program, Princess Margaret Hospital, University Health Network.

§ STTARR Innovation Centre, Radiation Medicine Program, Princess Margaret Hospital, University Health Network.

∥ Department of Radiation Oncology, University of Toronto.

⊥ Faculty of Pharmaceutical Sciences, University of Toronto.

(1) Allen, T. M.; Cheng, W. W.; Hare, J. I.; Laginha, K. M. Pharmacokinetics and pharmacodynamics of lipidic nano-particles in cancer. *Anticancer Agents Med. Chem.* **2006**, *6* (6), 513–523.

(2) Gabizon, A.; Tzemach, D.; Mak, L.; Bronstein, M.; Horowitz, A. T. Dose dependency of pharmacokinetics and therapeutic efficacy of pegylated liposomal doxorubicin (DOXIL) in murine models. *J. Drug Targeting* **2002**, *10* (7), 539–548.

(3) Cui, J.; Li, C.; Guo, W.; Li, Y.; Wang, C.; Zhang, L.; Hao, Y.; Wang, Y. Direct comparison of two pegylated liposomal doxorubicin formulations: is AUC predictive for toxicity and efficacy? *J. Controlled Release* **2007**, *118* (2), 204–215.

(4) Ishida, T.; Atobe, K.; Wang, X.; Kiwada, H. Accelerated blood clearance of PEGylated liposomes upon repeated injections: effect of doxorubicin-encapsulation and high-dose first injection. *J. Controlled Release* **2006**, *115* (3), 251–258.

10.1021/mp800234r CCC: $40.75 © **2009 American Chemical Society**
Published on Web 03/19/2009

alization of the spatial and temporal distribution of these agents through labeling with fluorescent, radioactive, radioopaque or paramagnetic molecules and assessment using optical, single photon computed tomography (SPECT), positron emission tomography (PET), CT and magnetic resonance imaging (MRI), respectively.[5−10] The noninvasive nature of image-based assessments allows for repeated *in vivo* and *in situ* data acquisition from the same subject over multiple time points, thereby reducing the required number of animals while increasing the accuracy of measurements. Furthermore, if a high resolution imaging technique is employed, the intraorgan and tissue distribution of the agent can be resolved. As a result, imaging has become utilized increasingly for biodistribution investigations; however, appropriate extraction of quantitative data from images still remains a challenge.

Nanosized lipid nanoparticles such as liposomes have been widely employed as delivery vehicles for a range of molecules such as drugs and contrast agents. Their size and surface properties have proven to be critical for passive accumulation in tumors and sites of inflammation through the enhanced permeation and retention (EPR) effect.[11−14] Their *in vivo* distribution has been assessed by numerous research groups in a variety of healthy and disease-bearing animal models as well as in patients using both traditional tissue extraction [15,16] and nuclear imaging techniques.[17,18] SPECT imaging techniques rely on radioisotope labeling of liposomes. As a result, the imaging time window is limited by the physical half-life of gamma photon emitting isotopes such as Tc^{99m} ($t_{1/2} = 6$ h) or In^{111} ($t_{1/2} = 67$ h), and increased image acquisition time is necessary to compensate for radioisotope decay. CT contrast agents such as iodine and barium are nonradioactive, have high atomic numbers and provide high X-ray attenuation. The employment of a CT-based assessment is therefore suitable for investigations involving long-circulating nanoparticle systems, as well as for monitoring slow physiological processes such as the passive accumulation of nanocarriers in tumors via the EPR phenomenon. Furthermore, volumetric CT imaging allows for extremely fast data acquisition in submillimeter isotropic voxels. When combined with 3D image analysis tools, volumetric quantification of signal profiles within an organ or tissue of interest is possible. This enables the performance of whole body mass balance calculations and quantification of intraorgan heterogeneity. In addition, CT is currently the fastest and most widespread whole body volumetric imaging modality, which makes it very attractive for high throughput biodistribution investigations.

The goal of the current research is to longitudinally quantify the presence of iohexol and gadoteridol-containing liposomes in the various body compartment volumes, as well as to visualize the heterogeneity of liposome distribution within a tumor using volumetric high-resolution CT imaging.

Experimental Section

Materials. The lipid components of the liposome bilayer 1,2-dipalmitoyl-*sn*-glycero-3-phosphocholine (DPPC, MW 734) and 1,2-distearoyl-*sn*-glycero-3-phosphoethanolamine-*N*-[poly(ethylene glycol)2000] (PEG_{2000}DSPE, MW 2774) were purchased from Genzyme Pharmaceuticals (Cambridge, MA); cholesterol (CH, MW 387) was purchased from Northern Lipids Inc. (Vancouver, British Columbia, Canada). The CT contrast agent Omnipaque (Nycomed Imaging AS, Oslo, Norway) has an iodine concentration of 300 mg/mL and consists of the nonionic, iodinated molecule iohexol (*N*,*N*′-bis(2,3-dihydroxypropyl)-5-[*N*-(2,3-dihydroxypropyl)-acetamido]-2,4,6-triiodo-isophthalamide, MW 821.14, 3 iodine atoms per molecule) dissolved in an aqueous solution with tromethamine and edentate calcium disodium. The nonionic, gadolinium complex gadoteridol (10-(2-hydroxypropyl)-1,4,7,10-tetraazacyclododecane-1,4,7-triacetic acid,

(5) Lu, Z. R.; Ye, F.; Vaidya, A. Polymer platforms for drug delivery and biomedical imaging. *J. Controlled Release* **2007**, *122* (3), 269–277.
(6) Koning, G. A.; Krijger, G. C. Targeted multifunctional lipid-based nanocarriers for image-guided drug delivery. *Anticancer Agents Med. Chem.* **2007**, *7* (4), 425–440.
(7) Tashjian, J. A.; Dewhirst, M. W.; Needham, D.; Viglianti, B. L. Rationale for and measurement of liposomal drug delivery with hyperthermia using non-invasive imaging techniques. *Int. J. Hyperthermia* **2008**, *24* (1), 79–90.
(8) Nasongkla, N.; Bey, E.; Ren, J.; Ai, H.; Khemtong, C.; Guthi, J. S.; Chin, S. F.; Sherry, A. D.; Boothman, D. A.; Gao, J. Multifunctional polymeric micelles as cancer-targeted, MRI-ultrasensitive drug delivery systems. *Nano Lett.* **2006**, *6* (11), 2427–2430.
(9) Mitra, A.; Nan, A.; Line, B. R.; Ghandehari, H. Nanocarriers for nuclear imaging and radiotherapy of cancer. *Curr. Pharm. Des.* **2006**, *12* (36), 4729–4749.
(10) Torchilin, V. P. Targeted pharmaceutical nanocarriers for cancer therapy and imaging. *AAPS J.* **2007**, *9* (2), E128−147.
(11) Hoffman, A. S. The origins and evolution of "controlled" drug delivery systems, *J. Controlled Release* **2008**, E-pub.
(12) Greish, K. Enhanced permeability and retention of macromolecular drugs in solid tumors: a royal gate for targeted anticancer nanomedicines. *J. Drug Targeting* **2007**, *15* (7−8), 457–464.
(13) Torchilin, V. P. Micellar nanocarriers: pharmaceutical perspectives. *Pharm. Res.* **2007**, *24* (1), 1–16.
(14) Iyer, A. K.; Khaled, G.; Fang, J.; Maeda, H. Exploiting the enhanced permeability and retention effect for tumor targeting. *Drug Discovery Today* **2006**, *11* (17−18), 812–818.
(15) Drummond, D. C.; Noble, C. O.; Hayes, M. E.; Park, J. W.; Kirpotin, D. B. Pharmacokinetics and in vivo drug release rates in liposomal nanocarrier development. *J. Pharm. Sci.* **2008**, *97* (11), 4696–4740.
(16) Vail, D. M.; Amantea, M. A.; Colbern, G. T.; Martin, F. J.; Hilger, R. A.; Working, P. K. Pegylated liposomal doxorubicin: proof of principle using preclinical animal models and pharmacokinetic studies. *Semin. Oncol.* **2004**, *31* (6 Suppl. 13), 16–35.
(17) Harrington, K. J.; Mohammadtaghi, S.; Uster, P. S.; Glass, D.; Peters, A. M.; Vile, R. G.; Stewart, J. S. Effective targeting of solid tumors in patients with locally advanced cancers by radiolabeled pegylated liposomes. *Clin. Cancer Res.* **2001**, *7* (2), 243–254.
(18) Goins, B. A.; Phillips, W. T. The use of scintigraphic imaging as a tool in the development of liposome formulations. *Prog. Lipid Res.* **2001**, *40* (1−2), 95–123.

MW 558.7, 1 gadolinium atom per complex, ProHance by Bracco Diagnostics Inc., Princeton, NJ) dissolved in an aqueous solution with calteridol calcium and tromethamine (gadolinium concentration of 78.6 mg/mL) was also encapsulated in the liposomes.

Preparation and Characterization of Liposome Formulations. The liposome composition (DPPC, cholesterol and $PEG_{2000}DSPE$ in 55:40:5% mole ratios) and preparation method were described in detail in previous publications.[19,20] The mean diameter of the final liposome sample was measured by dynamic light scattering (DLS) analysis of dilute solutions using a DynaPro DLS instrument (Protein Solutions, Charlottesville, VA) at 25 °C. The final concentration of iohexol was determined using a UV assay with detection at a wavelength of 245 nm (Cary 50 UV/vis spectrophotometer, Varian Inc., CA). The final concentration of gadoteridol was determined using an assay based on inductively coupled plasma atomic emission spectrometry (ICP-AES Optima 3000DV, Perkin-Elmer, MA).

CT Imaging of Tumor Bearing Rabbits. The following *in vivo* imaging study was performed under a protocol approved by the University Health Network Animal Care and Use Committee. Five healthy male New Zealand White rabbits (2.8−3.2 kg) were inoculated with approximately 400 μL of VX2 sarcoma cells which were obtained from two propagation rabbits. The tumor cells were injected intramuscularly into the animals' left lateral quadriceps. The contrast-enhanced imaging studies were performed seven to ten days after the tumor inoculation procedure. Specifically, each rabbit was intubated and kept under anesthesia with a mixture of isoflurane and oxygen via inhalation throughout each imaging session. A slow bolus injection (0.5 mL/s) of approximately 15 mL of the liposomal contrast agent formulation was then administered via the marginal ear vein catheter. Each rabbit received 1785 mg/kg of iohexol (equivalent to 276 mg/kg of iodine, corresponding to approximately half of the iodine dose/body weight typically administered to patients in a bolus form) and 40 mg/kg gadoteridol (equivalent to 11 mg/kg of gadolinium) coencapsulated within liposomes of 80.2 ± 3.4 nm in diameter and 6.2 ± 4.3% in polydispersity. CT Images (GE Discovery ST, General Electric Medical Systems, Milwaukee, WI) of the rabbits were acquired pre- and postadministration of the liposome formulation at 30 min as well as 1, 2, 3, 5, 7, 10 and 14 days following administration of the liposome formulation using the following imaging parameters: 80 kVp, 200 mA, a voxel size of 0.43 × 0.43 × 0.625 mm^3, and a FOV of 220 × 220 × 400 mm^3. The nominal X-ray dose for one whole body scan estimated by the scanner's CT dose index is 15 mGy. In addition, urine and feces samples were collected on a daily basis and analyzed for iodine content using neutron activation analysis (Becquerel Laboratories, ON, Canada) for assessment of liposome clearance route(s) and kinetics.

Volumetric Analysis of the CT Data Sets. Semiautomated contouring using MicroView v2.2 allowed for generation of three-dimensional volumes of interest consisting of the left and right kidneys, spleen, liver, tumor and the contra lateral muscle. The mean HU value for a given organ or tissue was calculated by averaging the signal of all voxels within the contoured volume. A voxel number versus CT signal profile was also generated for each volume at each imaging time point. All profiles were fit to a Gaussian curve with R^2 values greater than 0.90. The sigma of the signal profiles is a compounded result of the heterogeneity of the biological system and uncertainty in the measurement method. For the bulk volume analysis, an assumption was made that the organs and tissues of interest were homogeneous. The uncertainty in the measurement method was obtained by CT imaging a large water phantom and measuring the standard deviation of the signal within volumes of similar size as the organs and tissues of analysis (ranging from 0.2 to 40.9 cm^3). The Welch's *t*-test was used to calculate the degree of significance between the CT signals within the same organ over the different time points. The difference between the mean Hounsfield unit (HU) measured at time *t* post-liposome injection and the mean HU measured pre-liposome administration at time $t = 0$ (eq 1).

$$\Delta\text{meanHU} = \text{meanHU}_t - \text{meanHU}_{t=0} \qquad (1)$$

Results

Liposome Accumulation and Clearance Kinetics in Organs and Tissues of Interest. An axial image representing each organ and tissue of interest is shown in Figure 1a. In Figure 1b, the organ volumes that were contoured and analyzed are illustrated in yellow with respect to their locations within the rabbit body. The liposome accumulation and clearance kinetics profiles in each organ (left and right kidneys, liver, spleen and tumor) of each of the five animals are shown in Figure 1c as ΔmeanHU (eq 1).

In all volumes of interest and in all five animals, a sharp increase in the mean HU value was seen immediately following the administration of the liposome agent (30 min postinjection) as a result of the systemic distribution of liposomes in the blood stream. While the mean signal intensities measured in the healthy organs (kidneys, liver and spleen) decreased over time, significant contrast enhancement of the tumor volume is not observed until 24 h postinjection, and it is sustained up to 10 days following a single administration of the liposomes (Figure 2a). As a control, analysis was also performed on the muscle volume located on the contra-lateral thigh. The highest tumor-to-muscle iodine concentration ratio of 11.9 ± 6.0 was detected at 7 days postinjection (Figure 2b). However, the highest liposome accumulation (915 $\mu g/cm^3$ of iodine) at the tumor site occurred at 48 h following administration. The linear relationship between differential CT attenuation values and iodine concentration was determined in a

(19) Zheng, J.; Perkins, G.; Kirilova, A.; Allen, C.; Jaffray, D. A. Multimodal contrast agent for combined computed tomography and magnetic resonance imaging applications. *Invest. Radiol.* **2006**, *41* (3), 339–348.

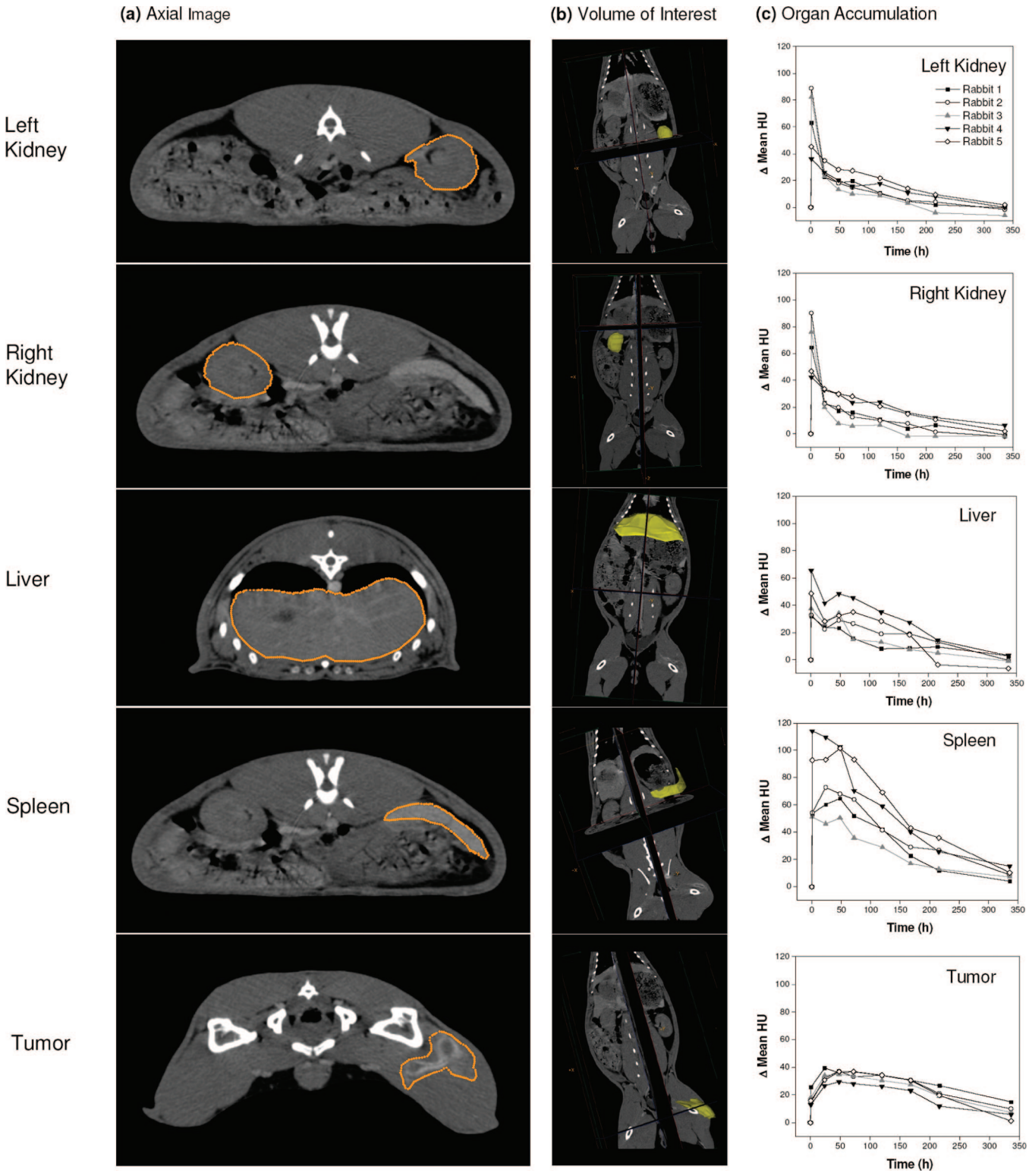

Figure 1. Visual illustration of (a) axial CT slices of the rabbit kidneys, liver, spleen and tumor acquired at 48 h postinjection. These images are acquired at submillimeter resolution, and they demonstrate potential for quantification of intraorgan heterogeneity. In this particular study, bulk organ analysis was performed on (b) the contoured organ/tissue volumes (in yellow). (c) The differential mean HU measured in each volume of interest (with respect to the preinjection data set) at selected time points. Each profile represents the values obtained for a given rabbit over 14 days.

separate phantom study. It was measured that every 1 mg/mL of iodine and 0.05 mg/mL of gadolinium encapsulated in liposomes provided a differential signal increase of 38.04 ± 0.64 HU in CT when operated at 80 kVp and 200 mA. The coefficient of determination R^2 for the linear regression was 0.996.

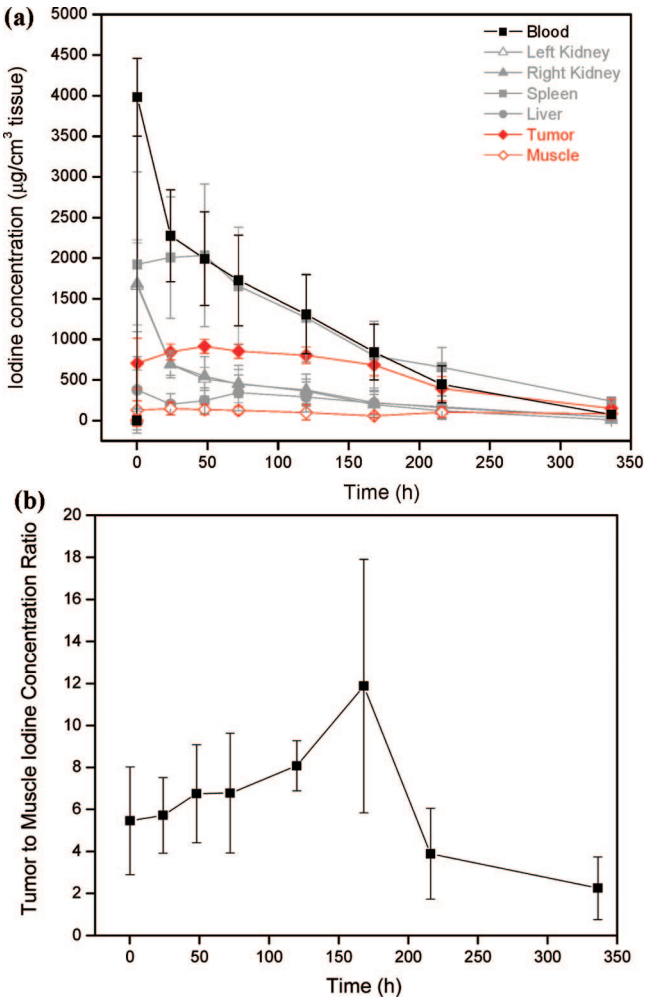

Figure 2. (a) Liposome biodistribution profiles in various organs and tissues of interest as measured using CT-based detection of the liposome-encapsulated iohexol and gadoteridol. The encapsulated iodine to gadolinium weight ratio is 20 to 1. At day 14, the blood, spleen, tumor and muscle showed statistically significant accumulation of liposomes ($p < 0.001$), while the mean signal measured in the kidneys and the liver was not statistically significant compared to the mean signal of the same organs pre-liposome administration. (b) Time-dependent tumor-to-muscle ratio of iodine concentration. The highest ratio occurs at 7 days post-liposome injection. Each data point represents the mean ± standard deviation for five animals.

Conventional biodistribution studies and nuclear medicine imaging techniques report the amount of drug or agent extracted or the total radioactivity measured from a given organ or tissue, respectively, as a percentage of the injected dose (% ID) and as percentage of the injected dose per weight (% ID/g or % ID/kg) of the organ or tissue of interest. This data is measured from the CT data set using an anatomically accurate volumetric organ-based analysis technique. Table 1 displays the percentage of injected iodine per organ and the percentage of injected iodine per volume (cm^3) of tissue for blood, kidneys, liver, spleen and tumor. Our findings are in agreement with a study performed by Harrington et al.[17] in cancer patients who had been administered ^{111}In-DTPA labeled Doxil liposomes and imaged with SPECT. It is important to note that there are physiological differences between rabbits and human. The lipid composition of the liposomes employed for this study (DPPC:cholesterol:PEG_{2000}DSPE at 55:40:5 mol %) is fairly similar to the Doxil liposome formulation (HSPC:cholesterol:PEG_{2000}DSPE at 56:39:5 mol %). Previously, our group has shown that the biodistribution profile of this liposome formulation in healthy mice matched the profiles reported by other groups who used either Doxil liposomes or other liposome formulations that closely matched the composition of Doxil.[20,21] Table 1 shows that the % ID of iodine measured in the rabbits' vascular compartment using CT is 89.8 ± 19.5% at 30 min postinjection and decreases to 51.4 ± 4.2% at 48 h and then to 10.9 ± 3.3% at day 10. In comparison, Harrington et al. reported that 95.0 ± 11.8% of the % ID of ^{111}In (i.e., ^{111}In-Doxil) remained in patients' blood 30 min post-liposome administration, 55.5 ± 9.3% at 48 h and 4.9 ± 5.1% at day 10. The blood pharmacokinetics profile from each rabbit was fitted to a one-compartment model, and the mean vascular half-life $t_{1/2}$ was calculated to be 63.6 ± 5.8 h. The R^2 values indicative of the goodness of fit ranged between 0.90 and 0.97 across the study population.

In addition, the liposome accumulation in each rabbit kidney was measured to be between 1.9 ± 0.5% (0.5 h) and 0.1 ± 0.1% (240 h), in agreement with the values reported by Harrington et al. of 1.6 ± 0.8% (0.5 h) and 0.7 ± 0.4% (240 h) in patients. As well, the tumor accumulation in rabbits was measured to be 0.9 ± 0.3% in this study at 72 h postinjection, which falls within the range of 0.3−2.6% ID reported for patients having different types of tumor burden and treated with Doxil liposomes. However, the % ID of liposomes measured in the rabbit liver and spleen was about four times lower than the values reported by Harrington et al. in patients. In fact, a greater degree of cumulative excretion via the urinary route was observed in the current study (27.0 ± 15.7% ID) compared to the 18.3 ± 6.9% ID reported by Harrington et al. over the first 4 days postinjection. Stool samples collected from all five animals over the entire study period revealed a cumulative 7.3 ± 9.8% ID of iodine excreted at day 4 and a cumulative 12.6 ± 15.1% ID excreted at day 14. Overall, with the combination of the CT volume analysis method for blood, kidneys, liver, spleen and tumor, and iodine detection in urine and feces, it was possible to account for 100.8 ± 22.0% of the total injected dose of iodine at 30 min post liposome administration, 80.8 ± 12.2% of the total injected dose at 72 h postinjection, and 58.5 ± 9.4% of the total injected dose at 14 days postadministration.

(20) Zheng, J.; Liu, J.; Dunne, M.; Jaffray, D. A.; Allen, C. In vivo performance of a liposomal vascular contrast agent for CT and MR-based image guidance applications. *Pharm. Res.* **2007**, *24* (6), 1193–1201.

(21) Charrois, G. J.; Allen, T. M. Drug release rate influences the pharmacokinetics, biodistribution, therapeutic activity, and toxicity of pegylated liposomal doxorubicin formulations in murine breast cancer. *Biochim. Biophys. Acta* **2004**, *1663* (1−2), 167–177.

Table 1. Liposome Biodistribution Expressed as % ID and as % ID/cm^3 of Organ/Tissue[a]

time (h)	blood	kidneys	liver	spleen	tumor	urine	feces
				% ID			
0.5	89.8 ± 19.5%	3.9 ± 0.6%	5.9 ± 2.7%	0.8 ± 0.5%	0.4 ± 0.1%	*b*	*b*
24	59.3 ± 4.7%	1.7 ± 0.4%	3.9 ± 0.9%	1.0 ± 0.4%	0.7 ± 0.1%	18.8 ± 14.3%	1.3 ± 1.7%
48	51.4 ± 4.2%	1.3 ± 0.4%	4.4 ± 1.0%	1.0 ± 0.4%	0.9 ± 0.3%	22.9 ± 16.2%	4.2 ± 6.0%
72	44.2 ± 5.9%	1.0 ± 0.4%	4.3 ± 2.8%	0.7 ± 0.3%	0.9 ± 0.3%	24.2 ± 16.9%	5.5 ± 7.5%
120	33.1 ± 4.8%	0.8 ± 0.3%	3.0 ± 2.2%	0.5 ± 0.2%	1.1 ± 0.3%	29.4 ± 14.8%	8.5 ± 10.7%
168	21.1 ± 4.5%	0.5 ± 0.3%	2.2 ± 1.5%	0.3 ± 0.2%	1.1 ± 0.3%	35.3 ± 14.9%	10.3 ± 12.7%
240	10.9 ± 3.3%	0.3 ± 0.2%	1.2 ± 0.8%	0.2 ± 0.1%	1.0 ± 0.3%	39.5 ± 13.9%	11.8 ± 14.3%
336	2.1 ± 1.4%	*c*	*c*	0.1 ± 0.0%	0.6 ± 0.3%	43.1 ± 12.3%	12.6 ± 15.1%
				% ID/cm^3			
0.5	0.42 ± 0.04%	0.20 ± 0.08%	0.14 ± 0.05%	0.24 ± 0.10%	0.05 ± 0.05%		
24	0.29 ± 0.06%	0.09 ± 0.02%	0.10 ± 0.03%	0.25 ± 0.08%	0.09 ± 0.02%		
48	0.25 ± 0.06%	0.07 ± 0.02%	0.11 ± 0.03%	0.26 ± 0.07%	0.11 ± 0.01%		
72	0.22 ± 0.06%	0.06 ± 0.02%	0.10 ± 0.04%	0.21 ± 0.06%	0.11 ± 0.01%		
120	0.16 ± 0.05%	0.05 ± 0.02%	0.07 ± 0.03%	0.16 ± 0.04%	0.11 ± 0.01%		
168	0.11 ± 0.04%	0.03 ± 0.02%	0.05 ± 0.02%	0.10 ± 0.03%	0.10 ± 0.01%		
240	0.06 ± 0.03%	0.02 ± 0.02%	0.04 ± 0.01%	0.08 ± 0.02%	0.08 ± 0.02%		
336	0.01 ± 0.01%	*c*	*c*	0.03 ± 0.01%	0.04 ± 0.02%		

[a] The volume of the organs and tissues of interest was measured using the CT data set with the exception of the blood compartment. The blood volume for each animal was calculated as the injected dose divided by the *y*-intercept of the monoexponential fit from the blood iodine concentration vs time profile. The estimation rather than measurement of blood volume increases the uncertainty associated with the % ID and as % ID/cm^3 values for the blood pool. The high variance in the blood iodine content at 30 min postinjection is likely due to inaccuracies associated with the timing of the imaging session. The values for urine and feces are cumulative. Each table entry represents the mean ± standard deviation for five animals. [b] No urine or stool output. [c] Iodine concentration in this organ for this time point was below the detection limit.

The remaining amount of iodine may be nonspecifically distributed in other body compartments that were not included in this analysis such as the skin, muscle, fat or the interstitial fluid space.

Sensitivity of CT in Detecting the Tissue Concentrations of Iodine-Labeled Liposomes. CT imaging was performed on all animals pre and post contrast administration at selected time points. As stated in the methods, volumes of interests were generated from semiautomatic contours. The voxel number versus CT signal profiles generated were then Gaussian fitted with R^2 greater than 0.95 for kidneys, liver, spleen and tumor and with R^2 greater than 0.90 for blood. The Welch's *t*-test was used between each pair of pre- and postinjection volume sets to determine whether their signal profiles were statistically different ($p < 0.001$). The critical *t* value of 3.291 was then used to calculate the minimum differential HU needed for a given pre- and postinjection data set pair to be determined to be statistically different. These values were then converted into μg/cm^3 of iodine concentration representing the minimum amount of iodine that CT is able to detect in the different organs (Table 2). It is worth noting that all voxels within the liver, kidneys, spleen and tumor were used in the analysis in order to maximize statistical power. However, it was not possible to contour all voxels occupied by blood. As a result, the sensitivity in detecting iodine concentrations in blood can be improved by increasing the volume of analysis. In this case, due to the high iodine content circulating in the bloodstream, even at day 14, the blood iodine concentration (76.6 ± 39.5 μg/cm^3) was above the limit of detection of the current method (11.4 μg/cm^3).

Table 2. List of the mean organ and tissue sampling volumes used during the analysis of the CT data sets. For a given body compartment of a set mean volume, the minimum mean differential HU (ΔHU) needed to detect statistically significant amounts of iodine was calculated using the Welch's *t*-test

	mean sampling volume (cm^3)	minimum mean ΔHU for significance ($p < 0.001$)	iodine detection sensitivity (μg/cm^3)
blood	0.2	0.68	11.4
kidney	9.0	0.10	1.6
liver	40.9	0.05	0.8
spleen	3.1	0.17	2.9
tumor	11.4	0.11	1.8

Classification of Heterogeneity in the Intratumoral Distribution of Liposomes. Once it had been established that the iodine detection sensitivity in the tumor is 1.8 μg/cm^3 (equivalent to a differential mean HU increase of 0.11 ΔHU) for this particular study, it was possible to calculate and visualize the percentage of tumor volume that was occupied by iodinated liposomes. Figure 3 provides visual illustration of the accumulation and clearance of the iodinated liposomes from the tumors of the five rabbits over the 14-day period. It may be noted that although the percentage of tumor volume occupancy by the liposomes is fairly consistent across the five data sets, the spatial distribution patterns differ significantly from animal to animal. The graph in Figure 4a shows the time dependent volume of distribution of liposomes in tumor as the fraction of the total tumor volume

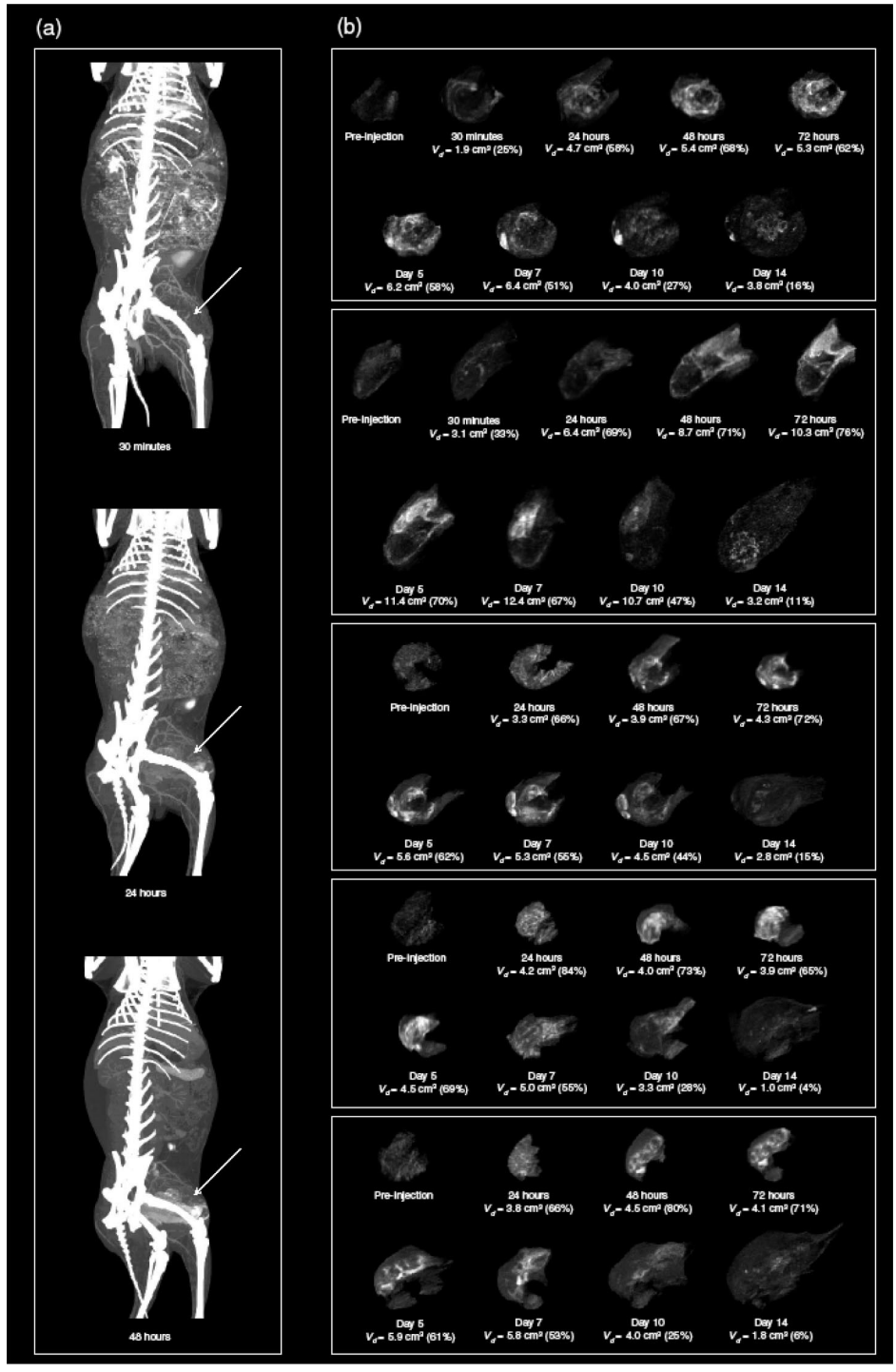

Figure 3. (a) Anterior views of 3D CT maximum intensity projections (MIP) of a representative VX2 sarcoma bearing male New Zealand White rabbit (3 kg) at 30 min, 24 and 48 h post liposome administration. The arrows indicate the site of the tumor, and the EPR effect is visualized through the gradual opacification of the tumor area resulting from the accumulation of the iohexol and gadoteridol containing liposomes. Adapted with permission from Zheng et al.[28] (Zheng, J.; Hoisak, J. D.; Allen, C.; Jaffray, D. A. Longitudinal Vascular Imaging Using a Novel Nano-encapsulated CT and MR Contrast Agent. *Proc. SPIE* **2007**, *6511*, 65111D-1, Medical Imaging 2007) to illustrate the anatomical location of the segmented tumor volumes. Copyright 2007 SPIE. (b) The five quadrants represent data acquired from five distinct animals, with each quadrant displaying 3D maximum intensity projections of the segmented tumor volumes pre and up to 14 days post liposome injection. Note that the tumor growth process can also be monitored, visualized and effectively measured using CT (see Figure 4b).

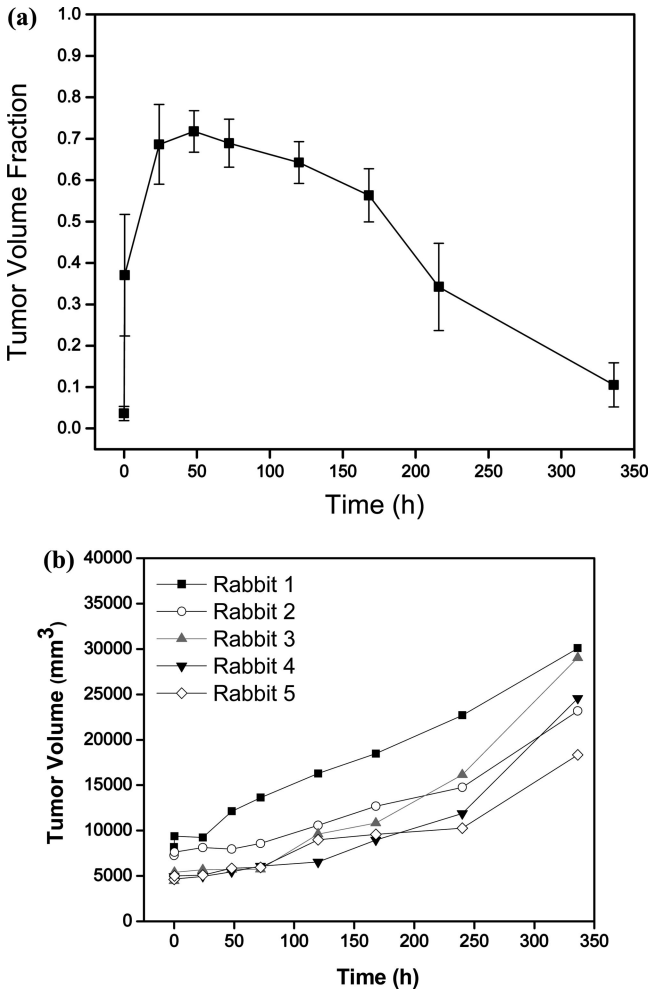

Figure 4. (a) Representation of the tumor volume fraction occupied by liposomes over 14 days. Voxels with values greater than or equal to the $\mu + 2\sigma$ of the preinjection tumor CT signal were considered contrast enhanced. Each data point represents the mean ± standard deviation for five animals. (b) Changes in tumor volume measured using CT in the five rabbits over 14 days.

occupied. The percent occupancy peaked at 72 ± 5% 48 h postinjection.

Discussion

Recent developments in image-guided drug delivery are prompted by the belief that an increased understanding of the biodistribution of drug carriers in individual patients will lead to improvements in personalized treatment design and delivery. Advances in nanosized drug carriers have enabled improved delivery of anticancer drugs to the tumor site, by exploitation of the EPR phenomenon, while minimizing their nonspecific distribution to healthy organs and tissues. EPR describes the mechanism by which macromolecules or nanoparticles are retained within healthy vasculature due to their colloidal size, but are able to accumulate in tumors due to the leakiness of the abnormal vasculature and lack of effective lymphatic drainage at these sites, in comparison to normal tissue.[11−14] The addition of an imageable component to a drug carrier, in combination with the employment of volumetric imaging techniques, enables noninvasive visualization and quantification of the effectiveness of tumor targeting and sparing of healthy tissue. The successful translation of image-guided drug delivery to the clinical setting would permit timely adjustments of treatment regimens on a per patient basis and ultimately enable implementation of personalized medicines.

In the current study, iohexol and gadoteridol were coencapsulated within liposomes to enable CT and MR imaging of the nanoparticle biodistribution following administration. The physicochemical characteristics and stability of this formulation have been described in detail elsewhere.[19] We also previously reported the pharmacokinetics profiles of iohexol and gadoteridol as free agents and liposome-encapsulated agents[20] to demonstrate the prolonged imaging window of the contrast agent encapsulated liposomes. Similar to other small molecules, unencapsulated iohexol and gadoteridol exhibit rapid distribution and clearance upon administration. Liposome encapsulation of the small molecular weight agents changed their profiles from biphasic to monophasic. In healthy Balb-C mice, the calculated $t_{\alpha 1/2}$ was 12.3 ± 0.5 min for iohexol and 7.6 ± 0.9 min for gadoteridol, and the elimination (β phase) half-lives were 3.0 ± 0.9 h for iohexol and 3.0 ± 1.3 h for gadoteridol; whereas the vascular half-lives were 18.4 ± 2.4 and 18.1 ± 5.1 h for iohexol and gadoteridol, respectively, when coencapsulated in liposomes.[20] As a result, it is reasonable to attribute the longitudinal signal increases observed in the blood and tissue compartments to the presence of the encapsulated agents.

Once it is established that the images are indeed reporting the biodistribution of the nanoparticulate carriers, there remains a significant challenge in using imaging techniques to assess the *in vivo* performance of drug delivery systems. This challenge lies in the accurate extraction of quantitative data from the images. First, it must be ensured that the given signal change measured in a given voxel corresponds to a consistent change in the concentration of the nanocarrier in the same volume. When using imaging modalities such as MR and CT, in which signal changes can occur as a result of endogenous changes in tissue properties, the benefit of having anatomical information comes with the challenge of extracting signal changes that are solely generated by the presence of contrast agents. For example, when conducting longitudinal studies lasting days to weeks in a tumor-bearing animal, the tumor morphology and physiology can change. The signal generation process of an anatomic MR data set relies on the tissue T1 and T2 relaxation parameters, which are known to be very sensitive to changes in tumor tissue properties such as local water concentration.[22] The sensitivity to these parameters, which have made MR so powerful for soft tissue and tumor characterization, increases the challenge of quantifying

(22) Pathak, A. P. Magnetic resonance imaging of tumor physiology. *Methods Mol. Med.* **2006**, *124*, 279–297.

relaxivity changes that are exclusively caused by shifts in the contrast agent concentration. The underlying signal generation process in CT is dependent on the X-ray attenuation profile of a tissue, which during disease progression undergoes a more gradual modification process than its relaxation properties. As a result, although the liposomes employed for this investigation coencapsulate iohexol and gadoteridol and can be imaged using both CT and MR, CT was relied on exclusively for quantification.

The second requirement for quantification of imaging data, in the case of a longitudinal study, is high confidence in defining corresponding volumes of interest for analysis across image sets acquired at different times. Although a voxel-based time-course analysis was not pursued here, both rigid and deformable image registration techniques have shown success, within a reasonable error range, in the identification of voxels across longitudinal data sets in organs and tissues that do not undergo significant anatomic changes over the course of the imaging study.[23,24] However, these algorithms cannot be applied to tissues that significantly change due to either disease progression or treatment. For example, during this particular study (2 weeks), the rabbit tumor volumes tripled in size (Figure 4b). Due to the low confidence in accurately identifying the same set of intratumoral voxels over time, a decision was made to measure the mean signal changes over all voxels that make up the bulk tumor volume and classify groups of intratumoral voxels according to their HU values rather than their spatial distribution (Figure 4a).

Finally, accurate quantification of the *in vivo* nanocarrier biodistribution is best achieved with a 3D analysis method. In situations when the nanocarrier is uniformly distributed, 2D ROI analysis may be preferred due to its simplicity and speed, and the mean signal value obtained is representative of the entire volume of interest. However, the nanocarrier distribution patterns are often heterogeneous or unknown, and the employment of 2D ROIs for image analysis is vulnerable to variations in 2D ROI placement. In this study, 3D ROI-based analysis was used on all organs and tissues of interest, whether or not they were known to be homogeneous or heterogeneous, in order to provide unbiased and observer-independent measurements that reflected the signal intensities of all voxels within the volumes of interest over all time points. The variance in the signal distributions provides insight on the heterogeneity of the organ/tissue under investigation. These heterogeneities include variance in anatomy, physiology and differential uptake and clearance of the contrast agent. The use of CT is attractive in monitoring these heterogeneities longitudinally due to its geometric accuracy. An additional advantage in using this 3D whole organ/tissue volume-based analysis is that it increased the number of voxels that were sampled for each measurement. As a result, a higher statistical confidence was achieved when comparing the differences among the signal profiles measured in the same organ or tissue over time, allowing us to confidently report much lower iodine concentrations (i.e., 0.8 μg/cm^3 for the liver, Table 2) compared to those published by other research groups that have employed 2D ROI analysis techniques.[25−27] This also demonstrates that there is an opportunity to decrease imaging dose while still satisfying the necessary level of iodine detection.

In conclusion, the feasibility and effectiveness of quantitative CT-based measurements of the pharmacokinetics and biodistribution of a nanocarrier *in vivo* have been demonstrated. Longitudinal imaging was performed up to 14 days post-liposome administration. The vascular half-life of 63.6 $\pm$ 5.8 h for the liposomes enabled high accumulation at the tumor sites (915 μg of iodine/cm^3 of tumor tissue at 48 h postinjection) through exploitation of the EPR effect. Furthermore, although the intratumoral distribution of liposomes was highly heterogeneous and variable from animal to animal, the vehicle occupied the majority (72 $\pm$ 5%) of the total tumor volume at 48 h postinjection in the five rabbits. These observations support ongoing efforts in our research laboratory to develop robust metrics for spatial classification of the heterogeneous intratumoral distribution patterns of nanocarriers. These, in conjunction with molecular imaging tracers that report the different properties of the tumor microenvironment (i.e., FAZA-PET, FMISO-PET), will become a powerful tool set to elucidate the ability of drug carriers to deliver therapeutic agents to various intratumoral regions that have distinct sensitivities to treatment. In addition, increased employment of noninvasive, quantitative image-guided pharmacokinetics and biodistribution assessments in the development and preclinical testing of novel nanocarriers has the potential to greatly facilitate their clinical translation. Conversely, the adoption of imageable nanotherapeutics in the clinical setting, along

(23) Brock, K. K.; Dawson, L. A.; Sharpe, M. B.; Moseley, D. J.; Jaffray, D. A. Feasibility of a novel deformable image registration technique to facilitate classification, targeting, and monitoring of tumor and normal tissue. *Int. J. Radiat. Oncol. Biol. Phys.* **2006**, *64* (4), 1245–1254.

(24) Hutton, B. F.; Braun, M. Software for image registration: algorithms, accuracy, efficacy. *Semin. Nucl. Med.* **2003**, *33* (3), 180–192.

(25) Mukundan, S., Jr.; Ghaghada, K. B.; Badea, C. T.; Kao, C. Y.; Hedlund, L. W.; Provenzale, J. M.; Johnson, G. A.; Chen, E.; Bellamkonda, R. V.; Annapragada, A. A liposomal nanoscale contrast agent for preclinical CT in mice. *AJR, Am. J. Roentgenol.* **2006**, *186* (2), 300–307.

(26) Kao, C. Y.; Hoffman, E. A.; Beck, K. C.; Bellamkonda, R. V.; Annapragada, A. V. Long-residence-time nano-scale liposomal iohexol for X-ray-based blood pool imaging. *Acad. Radiol.* **2003**, *10* (5), 475–483.

(27) Ford, N. L.; Graham, K. C.; Groom, A. C.; Macdonald, I. C.; Chambers, A. F.; Holdsworth, D. W. Time-course characterization of the computed tomography contrast enhancement of an iodinated blood-pool contrast agent in mice using a volumetric flat-panel equipped computed tomography scanner. *Invest. Radiol.* **2006**, *41* (4), 384–390.

(28) Zheng, J.; Hoisak, J. D.; Allen, C.; Jaffray, D. A. Longitudinal vascular imaging using a novel nano-encapsulated CT and MR contrast agent. *Proc. SPIE* **2007**, *6511*, 65111D.

with quantitative imaging systems and analysis tools, will positively impact therapy outcome through personalization of treatment delivery.

Acknowledgment. This work is funded in part by CIHR and OICR research grants, the Fidani Chair in Radiation Physics and the Grange Advanced Simulation Initiative. J.Z. is grateful for the CIHR Canada Graduate Scholarship. The authors would like to thank Dr. Ivan Yeung for providing the VX2 tumor model, Dr. Sandy Pang for helpful comments and discussions with regard to pharmacokinetics modeling and the University Health Network animal care staff for their technical services.

MP800234R